Fuel 214 (2018) 436–445

Contents lists available at ScienceDirect

Fuel

journal homepage: www.elsevier.com/locate/fuel

Full Length Article

Dynamic simulation of fluidized bed chemical looping combustion process with iron based oxygen carrier

Dora-Andreea Chisalita, Ana-Maria Cormos*

Babeş-Bolyai University, Faculty of Chemistry and Chemical Engineering, Arany Janos Street, No. 11, Postal code: RO-400084 Cluj-Napoca, Romania

ARTICLE INFO

Keywords:
Chemical looping combustion
Fluidized bed
Dynamic simulation

ABSTRACT

Chemical looping combustion is a promising energy conversion technology for fossil fuel combustion with inherent carbon dioxide separation and minimum energy losses. A full understanding of the dynamic behavior is of paramount importance to successfully implement this technology at commercial scale. In this work, a dynamic mathematical model has been developed to simulate interconnected fluidized bed reactors of a 1 MW_{th} syngas-based chemical looping combustion process with iron based oxygen carrier. The model consists of mass and energy balances equations as well as the equations that describe the hydrodynamics and heat transfer processes. The particles distribution inside the fluidized bed reactors is described by a 1.5-D hydrodynamic model. The model showed two zones in axial direction (an upper lean zone and a bottom dense zone) and a horizontal separation between core region and wall layer. Different heat transfer mechanisms have been taken into account: convection between gas phase and the oxygen carrier particles; convection of the moving particle phase with wall and radiation. The developed model was used to predict (in space and time): gas and solid velocity distribution, gas composition distribution, behavior of oxygen carrier, and temperature profiles inside the air and fuel reactor. The dynamic behavior of the chemical looping combustion process was studied by step and ramp input changes in the input gas flow rate.

1. Introduction

Towards a better understanding of the world's climate and of the long-term impact of climate change, significant progress has been made in the last decades. The Intergovernmental Panel on Climate Change (IPCC) [1] showed that "most of the observed increase in globally averaged temperatures since the mid-20th century is very likely due to the observed increase in anthropogenic greenhouse gas concentrations". H_2O, CO_2, CH_4, N_2O, CFCs and SF_6 are the main gases that contribute to global warming and CO_2 is the most prevalent of greenhouse gases. The main sectors that contribute the most to global greenhouse gas emissions are: heat & power, industry, building, transport, agriculture, forestry and waste management. The energy sector causes the most of greenhouse gas emissions (in Europe, fuel combustion and fugitive emissions from fuels represented 55% of the greenhouse gas emissions, in 2014). Several options are investigated for mitigating CO_2 from the energy sector: renewables, nuclear, low carbon content fuel, increasing the efficiency of the fuel conversion and CO_2 capture and storage.

The renewable energy sources (e.g. biomass, solar, wind) due to their higher cost, are not yet competitive with fossil fuels in current market conditions. Nuclear energy faces barriers such as uncertainty regarding long term waste management, safety issues and adverse public opinion. Hence, fossil fuels will remain the major energy resource for the next decades and the use of coal will increase according to projections from the International Environmental Agency (IEA). Carbon Capture and Storage (CCS) seems to be a very promising method to significantly decrease CO_2 emissions from coal fired power plants. Different carbon dioxide capture techniques are currently investigated: pre-combustion, in which the fuel is decarbonized prior to combustion; oxy-fuel combustion, which uses nearly pure oxygen and post-combustion, which separate CO_2 form the flue gases using different approaches. All these carbon-capture techniques are energy intensive, resulting in increased fuel needs for coal fired power plants by 25–40%, and an increase of the energy production by 21–91% [2]. Considering all these factors a new technology, Chemical Looping Combustion (CLC), was proposed to increase thermal efficiency in power plants. CLC has the potential to be one of the most efficient and low cost technologies, with inherent advantages for CO_2 separation [3].

Chemical looping combustion involves the use of a metal oxide as an oxygen carrier (OC). The oxygen carrier makes a closed cycle between two interconnected reactors: in the fuel reactor the fossil fuel

* Corresponding author.
E-mail address: cani@chem.ubbcluj.ro (A.-M. Cormos).

https://doi.org/10.1016/j.fuel.2017.11.025
Received 29 April 2017; Received in revised form 11 October 2017; Accepted 7 November 2017
Available online 22 November 2017
0016-2361/

Nomenclature

A_0	area of distributor plate per orifice, m^2/orifice
A_B	cross sectional area of bed, m^2
A_p	heat transfer area of bed, m^2
C_g	reactive gas concentration, mol/m^3
F_j	gas/solid mass flow, kg/s
G_s	solid circulation rate, kg/(m^2·s)
G_s^*	saturated flux of solids out of reactor, kg/(m^2·s)
H_{dz}	dense zone height, m
H_{pg}	particle-gas heat flux, kJ/m^3·s
H_{pw}	particle-wall heat flux, kJ/m^3·s
H_r	heat of reaction, kJ/m^3·s
N_t	number of orifices in the distributor, -
Re_{mf}	minimum fluidization Reynolds number, -
U_0	superficial gas velocity, m/s
U_{br}	bubble riser velocity, m/s
U_g	total gas flow, m/s
U_{mf}	minimum fluidization velocity, m/s
U_t	terminal velocity, m/s
U_{tf}	gas throughout flow, m/s
U_v	visible bubble flow, m/s
X_{OC}	oxygen carrier conversion, -
a_d	decay factor, 1/m
d_b	bubble diameter, m
d_{b0}	initial bubble size, m
d_{bm}	maximum bubble diameter, m
d_p	particle diameter, m
k_S	kinetic constant, 1/s
x_i	component fraction, -
ΔP	pressure drop, kPa
h	height above the bottom of the bed, m
h_{pg}	particle-gas heat transfer coefficient, kW/m^2·K
h_{pw}	particle-wall heat transfer coefficient, kW/m^2·K
h_r	radiative heat transfer coefficient, kW/m^2·K
A	cross sectional area of bed/reactor, m^2
Ar	archimedes number, -
Cp	specific heat, kJ/kg·K
M	molecular mass, g/mol
Pr	Prandtl number: $Pr = Cp \cdot \mu / k$, -
R	ideal gas constant = 8.314, J/mol·K
S	heterogeneous reaction source term, kg/s·m
T	Temperature, K
	volumetric concentration of bed particles in the dispersed phase, %
e	emissivity, -
f	function, -
g	gravitational acceleration constant, m/s^2
k	thermal conductivity, -
m	mass load, kg
z	height of vertical position in the reactor, m

Greek letters

α	stoechiometric coefficient of components, -
β	stoechiometric coefficient of solid components, -
δ_b	volumetric fraction of bubbles, -
δ_w	thickness of annulus zone, m
ε_b	average bed porosity at a fixed position in the bottom bed, -
ε_{dz}	dense zone voidage, -
ε_e	emulsion voidage, -
ε_{mf}	porosity at minimum fluidization conditions, -
$\varepsilon_{s,dz}$	solid fraction/concentration in the dense zone, -
ε_s	solid fraction/concentration in the reactor, -
ε_s^*	saturation carrying capacity of gas, -
ρ_g	gas density, kg/m^3
ρ_p	particle density, kg/m^3
μ	gas viscosity, Pa·s
σ	Stefan-Boltzmann constant = 5.6703e−8, W/m^2 K^4
τ	reaction time, s
ψ	ratio of the visible bubble flow to the total flow through the bubbles, -
ϕ	sphericity -

Subscripts

dz	dense zone
g	gas
i	component
p	particle
s	solid
tz	transport zone
w	wall
c	cluster
l	lean particle phase

combustion takes place using the lattice oxygen of the metal oxide and in the air reactor the oxygen carrier is regenerated by oxygen from air. Therefore, CLC technology avoids direct contact between fuel and air and presents inherent sequestration of CO_2 without additional energy consumption. Complete combustion in the fuel reactor produces only CO_2 and water vapor. The outlet gas stream of the air reactor contains nitrogen and unreacted oxygen.

The overall reaction in the fuel reactor is the following:

$$(2n + m)M_yO_x + C_nH_{2m} \rightarrow (2n + m)M_yO_{x-1} + mH_2O + nCO_2$$

The OC is reoxidized, in the air reactor, according to the following reaction:

$$M_yO_{x-1} + 1/2O_2 \rightarrow M_yO_x + (N_2 + \text{unreacted}O_2)$$

In order to be used in a CLC process, the oxygen carrier should meet the following criteria: to be environmentally friendly, to have satisfactory thermodynamic properties for fuel conversion, to have high reactivity in both process steps (oxidation and reduction), low attrition as to be used in reasonable number of cycles, to have high melting points, low agglomeration tendency, mechanical strength in order to be able to be processed at desired particle size and to be economically feasible. Different types of oxygen carriers (e.g. Ni, Cu, Fe, Mn, Co-based oxides) should fulfill the above desired characteristics. Pure metal oxides, metal oxides mixed with supports (e.g. Al_2O_3, SiO_2, TiO_2, or ZrO_2) or combinations of metal oxides have been tested to get the desired properties [2,4]. The Fe-based oxygen carriers are suitable for chemical looping combustion applications because they are environmentally friendly, non-toxic for nature, less susceptible to carbon formation and have a good reactivity. Since iron ores occur naturally (such as magnetite, hematite, ilmenite, limonite, etc.), Fe-based oxygen carriers are inexpensive. The oxygen carrier used in this work is activated ilmenite. According to literature, ilmenite's reactivity increases after a number of 5–20 redox cycles, after which the reactivity remains mostly constant, so the activation process is relatively fast and can be done inside the chemical looping process [5].

The chemical looping process can be used either with gas, liquid or solid fuel, in the combustion step. In CLC of gaseous fuels, the oxygen carrier reacts directly with the primary fuel (e.g. natural gas, refinery

gas, syngas etc.). In case of natural gas and syngas a complete combustion has been obtained for different experimental conditions with Ni-, Cu-, Fe- and Mn-based materials [6]. The solid fuel (e.g. coal, biomass, pet-coke etc.) reacts directly or indirectly with oxygen carriers. There are two types of direct process: In-situ Gasification Chemical Looping Combustion (IG-CLC) and Chemical Looping with Oxygen Uncoupling (CLOU). In IG-CLC process, the solid fuel is gasified inside the fuel reactor and the products react with the oxygen carrier. In CLOU, the oxygen carrier releases gaseous oxygen in the fuel reactor, which carries out the combustion of the fuel. In case of indirect process, the solid fuel is converted in a gasifier and the syngas produced is introduced in the CLC system. For CLC with liquid fuel, limited studies have been reported in literature [2]. However, the use of liquid residues produced during refining of crude oil is the main goal for future work.

On the basis of reactor design, the chemical looping combustion process, can be configured in two interconnected moving or fluidized bed reactors; alternately packed or fluidized bed reactor and rotating reactors [2]. The two interconnected fluidized-bed reactors configuration, which consists of a high velocity riser (as air reactor) and a low / high velocity fluidized bed (as fuel reactor), is the most common and used configuration among all the different types [4]. In this configuration, a good mixing of gas and the solid carrier is provided and the circulation and replacement of the carrier material becomes easy. The solid particles leaving the air and fuel reactors are recovered by a cyclone and sent back to the fuel and air reactor respectively. Two loop-seal devices [7] placed between the air/fuel reactor and the cyclones prevent gas mixing between the two reactors. A schematic diagram of the syngas chemical looping combustion process is presented in Fig. 1.

A full understanding of the dynamic behavior is of paramount importance to successfully implement this technology at commercial scale. Mathematical modeling and simulation are modern assessment tools to be used in the development and deployment of chemical looping combustion technologies. The models must be able to describe the behavior of the gas–solid interactions inside the reactors and the dynamic behavior of interconnected fluidized columns. The available mathematical models of chemical looping combustion process are based on semi-empirical correlations or computational fluid dynamic technique [2]. Most of the computational fluid dynamic studies analyze the fuel reactor performance. The dynamic 1-D semi-empirical models available, describe CLC process with Ni/Cu based oxygen carriers in fluidized or fix bed reactors. The models showed good agreement with experimental results and were able to describe the process accurately. The main outputs of the models were the solids circulation rate, axial distribution of gas composition, temperature, oxygen carrier and reaction rate. Few modeling studies are available, in literature, in case of ilmenite as oxygen carrier. Parker (2014) [8] carried out a 3-D CFD simulation of the fuel reactor (on the bubbling bed regime) and air reactor (on fast fluidized bed regime). The circulation rate, reactor efficiencies and temperature profiles were predicted from the simulation results. Abad et al. (2013) [9] had developed a semi-empirical model for the fuel reactor (at high velocity fluidized regime). Based on the developed model, the axial profile of gas and solid compositions and the conversion of oxygen carrier and char inside the reactor were predicted.

This paper is assessing the performances of a 1 MW_{th} syngas chemical looping combustion system in a dynamic operation scenario. The operational parameters, the geometry of the fluidized bed reactors and the physical-chemical properties of the oxygen carrier (activated ilmenite) and gas phase (air and syngas) are the input parameters for the model. In this work, a new hydrodynamic model (1.5 D model) was implemented in order to describe the horizontal separation between core region and wall layer together with solid distribution in axial direction. The fluidized bed dynamics strongly influence the heat transfer, as a consequence different heat transfer mechanisms have been taken into account: convection between gas phase and the oxygen carrier particles; convection/conduction with the moving particle phase and radiation.

The developed dynamic model is used to predict the following parameters: gas and solid velocity distribution, gas composition distribution, properties and behavior of oxygen carrier, solid holdup and temperature profiles, in time, inside the air and fuel reactor. The oxygen carrier recovery rate has been studied during a ramp and step input tests to highlight the transient response of interconnected fluidized beds of the chemical looping system. The insights obtained from the dynamic simulation results are particularly useful for designing an advanced control scheme and for the evaluation of various operating conditions for chemical looping combustion optimization.

2. Model development

In a previous paper [10], a theoretical model, implemented in MATLAB/Simulink, describing the air and fuel reactors of a CLC system using methane and syngas as fuels was presented. An overview of the mass and energy balance equations is given in Table 1. The hypothesis considered for describing the complex heterogeneous phenomena are: (i) perfectly spherical solid particles with constant diameter and macroscopic properties; (ii) pseudo-homogeneous system within the elementary segment “dz”; (iii) plug-flow of gas and solid in both reactors. The developed model has the purpose of describing the behavior of both air and fuel reactors as fluidized bed reactors working at high-velocity regime. In the current work, the hydrodynamic model has been improved as well as the heat transfer mechanism (in previous work [10], a global heat transfer coefficient was used) which will be described in the following sections. As a new approach the models of air and fuel reactor have been interconnected.

The operating and design parameters used were based on a 1 MW_{th} CLC unit operated at TU Darmstadt, Germany [9,11] and are listed in Table 2.

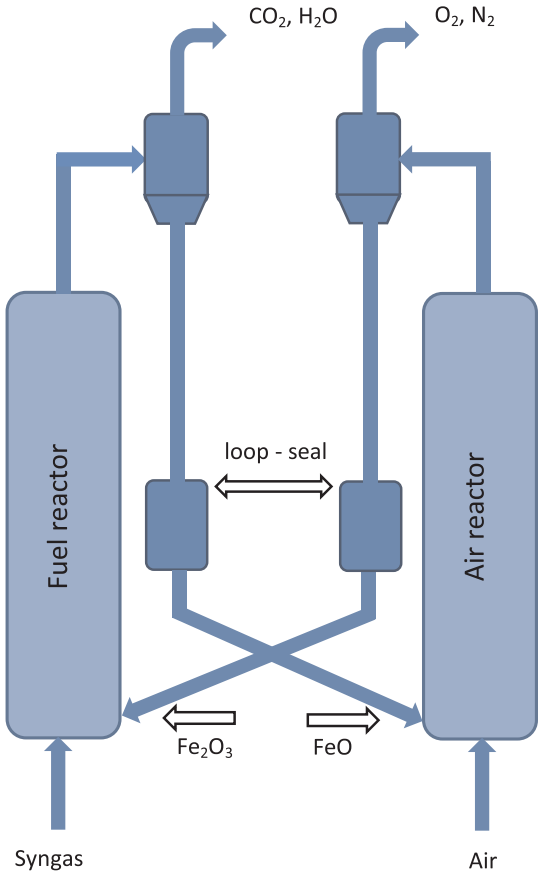

Fig. 1. Diagram of chemical looping process.

Table 1
Model equations [10].

Total mass balance [kg/m·s]

$$\frac{1}{U_j}\cdot\frac{\partial F_j}{\partial t} = -\frac{\partial F_j}{\partial z} \pm S\cdot\frac{\alpha\cdot M_i}{\beta\cdot M_{FeO/Fe_2O_3}}$$

Component mass balance [kg$_i$/m·s]

$$\frac{1}{U_j}\cdot\frac{\partial (F_j\cdot x_i)}{\partial t} = -\frac{\partial (F_j\cdot x_i)}{\partial z} \pm \sum S\cdot\frac{\alpha\cdot M_i}{\beta\cdot M_{FeO/Fe_2O_3}}$$

Energy balance [kJ/m^3·s]

$$\frac{1}{U_j}\cdot\frac{\partial (F_j\cdot Cp_j\cdot T_j)}{\partial t} = -\frac{\partial (F_j\cdot Cp_j\cdot T_j)}{\partial z} - (\Delta H_r\cdot S\cdot\frac{1}{M_{FeO/Fe_2O_3}}\cdot\frac{1}{A_p}) \pm H_{pg} - H_{pw}$$

Heterogeneous reaction source term [kg/m·s]

$$S = \frac{v_p\cdot F_{oc}}{w_s}$$

Table 2
Design and operating parameters [9,11].

Parameter	Unit	Air Reactor	Fuel Reactor
Height, H	m	8.7	11.4
Diameter, D	m	0.59	0.4
Fluidizing gas	–	Air	Syngas
Superficial gas velocity, U_0	m/s	3–3.5	3–3.5
Solid circulation rate, F_{OC}	kg/s	0.55–2.5	0.55–2.5
Pressure drop, ΔP	kPa	20	20
Oxygen carrier	–	Ilmenite	
Particle diameter, d_p	μm	250	
Apparent density, ρ_p	kg/m^3	3710	

2.1. Kinetics and thermodynamic aspects

Oxidation and reduction mechanisms of ilmenite are somewhat complex, depending on the thermodynamic conditions of the reaction.

Based on thermodynamic calculations, different studies [12–13] show that at temperatures higher than 853 K, pseudobrookite (Fe_2TiO_5) and rutile (TiO_2) are the preferred end-products of ilmenite oxidation. On the other hand, experimental data [14] showed that pseudobrookite was the only end-product when oxidation was carried out at temperatures greater than 1123 K and at lower temperatures a mixture of different compounds can be found. Taking all this into account, ilmenite oxidation's end-product can be considered as a mixture of Fe_2TiO_5, Fe_2O_3 and TiO_2 depending on temperature and reaction time:

$$2FeTiO_3 + 1/2O_2 \rightarrow Fe_2O_3{\circ}TiO_2 + TiO_2 \rightarrow Fe_2O_3 + 2TiO_2 \quad \text{(R1)}$$

$$3FeTiO_3 + 3/4O_2 \rightarrow Fe_2Ti_3O_9 + 1/2Fe_2O_3 \rightarrow 3/2Fe_2TiO_5 + 3/2TiO_2 \quad \text{(R2)}$$

At 973 K, Fe_2O_3 is separated from the titanium-rich phase, preventing the formation of Fe_2TiO_5 resulting thus in an increase of the Fe_2O_3 amount after every redox cycle as observed in more recent experimental results published by Adanez (2010) [15].

As the separate contribution of the reduction of Fe_2TiO_5 and Fe_2O_3 was not possible from the thermogravimetric analysis [16], for the reduction of ilmenite, the Integrated Rate of Reaction (IRoR) as described by Donski (2003) [17] was used. The IRoR model is widely used for the analysis of reduction of iron ores, considering pseudobrookite to be Fe_2O_3 + TiO_2, ilmenite as FeO + TiO_2 and magnetite as Fe_2O_3 + FeO, while TiO_2 is considered inert.

In the end, the oxidation and reduction of ilmenite with oxygen and coal derived syngas respectively, were expressed in a simplified manner in reactions (R3)–(R6) where all the ferric and ferrous components are represented by Fe_2O_3 and FeO respectively [16]. It can be noted that the oxidation reaction is exothermic while the reduction is endothermic, in this way, as the oxygen carrier circulates between the two reactors it also acts as heat transporter from the air reactor to the fuel reactor.

Table 3
Kinetic equations and parameters [16]

Equations	$\frac{dX_{OC}}{dt} = [\frac{3}{\tau}\cdot(1-X_{OC})^{\frac{2}{3}}]$	$\tau = \frac{\rho_m\cdot r_g}{\bar{b}}\cdot k_s\cdot C_g^n$		$k_S = k_{S0}\cdot e^{-E_a/RT}$
Parameters	Oxidation	Reduction		
	O_2	CH_4	H_2	CO
Molar density, $\rho_m[mol/m^3]$	31100	13590		
Grain radius, $r_g[m]$	1.2e−6	1.25e−6		
Average stoechiometric coefficient, $\bar{b}$	4	5.78	1.45	1.45
Pre-exponential factor, $k_{S0}[mol\cdot m/s]$	1.9e−2	9.8	6.2e−2	0.1
Activation energy, $E_a[kJ/mol]$	24.3	129.3	62.3	78.3
Reaction order, n	1	1	1	0.8

Air Reactor: $4FeO + O_2 \rightarrow 2Fe_2O_3 \quad \Delta H_r^{1323\,K} = -517.85\,[kJ/mol]$ (R3)

Fuel Reactor: $Fe_2O_3 + CO \rightarrow 2FeO + CO_2 \quad \Delta H_r^{1223\,K} = 25.83\,[kJ/mol]$ (R4)

$$Fe_2O_3 + H_2 \rightarrow 2FeO + H_2O \quad \Delta H_r^{1223K} = -7.86\ [kJ/mol] \quad \text{(R5)}$$

$$4Fe_2O_3 + CH_4 \rightarrow 8FeO + CO_2 + 2H_2O \quad \Delta H_r^{1223\,K} = 307.2\ [kJ/mol] \quad \text{(R6)}$$

The kinetic model used to describe the oxidation and reduction of ilmenite was the one proposed by Abad (2011) [16] which assumes that the oxygen carrier particle consists of a number of spherical, nonporous grains with uniform initial radius. The reaction takes place in the grain following the shrinking core model. The equations and the kinetic parameters used to describe the oxidation/reduction of ilmenite are summarized in Table 3.

2.2. Hydrodynamics

In a previous work [10], a 1-D hydrodynamic model developed by Kunii and Levenspiel [18] was used to describe the particle distribution inside the fluidized beds. In the present work a 1.5-D model was implemented in which the model is solved mainly in an axial direction with horizontal separation between core region and wall layer. Based on the solid fraction profiles, the fluidized bed can be divided into two zones: dense zone and upper zone. The dense zone is characterized by a relatively constant solid concentration while the upper zone is characterized by a decrease of the solid concentration with the height of the reactor.

The dense zone can be modeled according to the two phase flow theory described by Johnsson et el. (1991) [19] which describes the bed expansion of freely bubbling fluidized beds. The bed porosity and the solid fraction in the dense bed can be calculated from Eqs. (1) and (2):

$$\varepsilon_{dz} = \delta_b + (1-\delta_b)\cdot\varepsilon_{mf} \quad (1)$$

$$\varepsilon_{s,dz} = 1-\varepsilon_{dz} \quad (2)$$

From Kunii and Levenspiel (1991) [20] the values of solid fraction, $\varepsilon_{s,dz}$ for various fluidization regimes can be compared as follows:

Bubbling bed: $\varepsilon_{s,dz} = 0.55-0.40$
Turbulent bed: $\varepsilon_{s,dz} = 0.40-0.22$
Fast fluidization: $\varepsilon_{s,dz} = 0.22-0.16$

Bed porosity at minimum fluidization conditions can be calculated using the relation proposed by Broadhurst and Becker (1975) [21]:

$$\varepsilon_{mf} = 0.586\cdot\phi^{-0.72}\cdot Ar^{-0.029}\cdot\left(\frac{\rho_g}{\rho_p}\right)^{0.021} \quad (3)$$

The bubble fraction in the dense bed can be evaluated with Eq. (4):

$$\delta_b = \frac{1}{1+\frac{U_{br}}{U_v}} \quad (4)$$

where

$$U_{br} = 0.71\cdot\sqrt{g\cdot d_b} \quad (5)$$

$$U_v = \psi\cdot(U_0-U_{mf}) \quad (6)$$

The visible bubble flow U_v, is calculated as a function of a dimensionless visible bubble flow as described in Eq. (7):

$$\psi = f\cdot(h+4\cdot\sqrt{A_0})^{0.4} \quad (7)$$

where $f = [0.26+0.7\cdot exp(-3.3\cdot d_p)]\cdot[0.15+(U_0-U_{mf})]^{-0.33}$ with d_p expressed in [mm].

Based on experiments, several correlations have been developed for the estimation of the bubble growth in fluidized beds. In Kunii and Levenspiel (1991) [20], the bubble size d_b at any height, z, in the bed is given by the following expression:

$$\frac{d_{bm}-d_b}{d_{bm}-d_{b0}} = e^{-0.3\cdot\frac{z}{D}} \Rightarrow d_b = d_{bm}-(d_{bm}-d_{b0})\cdot e^{-0.3\cdot\frac{z}{D}} \quad (8)$$

The initial bubble size, d_{b0} depends on the type of gas distributor: perforated plate or porous plate [22]. In the present work perforated plate gas distributor was considered with 20 orifices for fuel reactor [9] and 30 for air reactor:

$$d_{b0} = 1.38\cdot g^{-0.2}\cdot\left[\frac{A_B\cdot(U_0-U_{mf})}{N_t}\right]^{0.4} \quad (9)$$

$$d_{bm} = 2.59\cdot g^{-0.2}\cdot[A_B\cdot(U_0-U_{mf})]^{0.4} \quad (10)$$

The solid fraction in the upper zone is divided into two phases: a splash phase and a transport phase. The splash phase is formed by the eruption of bubbles at the surface of the dense zone, being characterized by a strong back mixing of particles. Above the splash zone, a transport phase forms with a core-annulus structure being characterized by a more disperse-phase zone. Here, the particles are transported from the core to the wall layer where the gas velocity is significantly lower and the particles either fall down to the bottom bed or are entrained up through the transport zone [23].

The solid fraction in the upper zone, ε_s, can be evaluated using the relationship proposed by Zenz and Wein (1958) [24] which was shown to be valid for Dual Fluidized Bed Gasifiers (DFBG) by Loffler et al. (2003) [25]:

$$\frac{\varepsilon_s-\varepsilon_s^*}{\varepsilon_{s,dz}-\varepsilon_s^*} = e^{-a_d\cdot(H-H_{dz})} \quad (11)$$

Loffer et. al. (2003) [25] conducted a study to validate different correlations for the decay factor, a_d, on some experimental data and found that the empirical correlation proposed by Adanez (1994) [26] (Eq. (12)) is valid for operating conditions of 900 °C and superficial gas velocities between 2.9 and 5.1 m/s.

$$a_d\cdot(U_0-U_t)^2\cdot D^{0.6} = 3.5-1670\cdot d_p \quad (12)$$

The solid fraction in the dense bed was described earlier in Eq. (2). For the expression of the solid fraction at the exit or also known as saturation carrying capacity of gas, ε_s^*, the following relationship can be used [27]:

$$\varepsilon_s^* = \frac{G_s^*}{\rho_p\cdot(U_0-U_t)} \quad (13)$$

For a bed containing a single size of particles that are elutriable, the saturated flux of solids out of the reactor, G_s^*, can be expressed based on experimental correlations using Eq. (14) [20]. The most important parameters to check are the size range of particles as well as the gas velocity. In this case, the experimental conditions under which the relationship is valid are: $d_p = 60-300[\mu m]$, $U_0 = 0.6-3[m/s]$.

$$G_s^* = 23{,}7\cdot\rho_g\cdot U_0\cdot exp\left(-5{,}4\cdot\frac{U_t}{U_0}\right) \quad (14)$$

Using the saturated flux of solids G_s^*, instead of the solid circulation rate G_s, the solid velocity obtained in saturated conditions should be overestimated [22]:

$$U_s = \frac{G_s^*}{\rho_p\cdot\varepsilon_s} \quad (15)$$

The height of the dense zone can be expressed out of the pressure drop along the columns. The height is obtained by iteration until the pressure drop converges according to Eqs. (16)(18).

$$\Delta P_{dz} = \rho_p\cdot\varepsilon_{s,dz}\cdot g\cdot H_{dz} \quad (16)$$

$$\Delta P_{tz} = \rho_p\cdot\varepsilon_s\cdot g\cdot(H-H_{dz}) \quad (17)$$

$$\Delta P_{AR} = \Delta P_{dz}+\Delta P_{tz} \quad (18)$$

Similarly, the amount of bed material at any height is given by the following relations:

$$m_{dz} = A\cdot\rho_p\cdot\varepsilon_{s,dz}\cdot H_{dz} \quad (19)$$

$$m_{tz} = A\cdot\rho_p\cdot\varepsilon_s\cdot(H-H_{dz}) \quad (20)$$

2.3. Heat transfer

The bed fluid dynamics, as well as the particle properties and operating conditions strongly influence the heat transfer coefficients [28]. As described in Section 2.2, the bed hydrodynamics have a core-annulus structure with particles forming packets or clusters near the wall which travels downward for certain distance and then disintegrate and reform again, while in the core, gas will flow upwards with more diluted particles. Different heat transfer mechanisms should be taken into account when dealing with fluidized bed systems, namely: (i) convection between gas phase and the oxygen carrier particles; (ii) convection/conduction with the moving particle phase; (iii) radiation. A schematic representation of the forming and disintegration of clusters near the wall as well as the heat transfer mechanisms taking place at the wall are presented in Fig. 2.

In describing the particle-gas heat flux (Eq. (21)), Makkawi (2013) [31] proposes a relationship for the convective heat transfer between particles and gas that takes into account the particle velocity, concentration and length of the heat transfer section which is described in Eq. (22):

$$H_{pg} = h_{pg}\cdot a\cdot(T_p-T_g) \quad (21)$$

$$h_{pg} = 8.4\cdot Re_p^{0.871}\cdot\left[\frac{(1-\varepsilon)\cdot z}{d_p}\right]^{0.924} \quad (22)$$

With $Re_p = \frac{\rho_g\cdot U_s\cdot d_p}{\mu}$ valid for $0.1 < Re_p < 200$ and $\varepsilon > 0.8$.

The bed voidage, or in other words the volume fraction of the bed occupied by bubbles, can be assessed using Eq. (23) [32]:

$$\varepsilon = 1-\frac{\Delta P}{H\cdot(\rho_p-\rho_g)\cdot g} \quad (23)$$

For spherical particles, the particle surface area per unit volume can

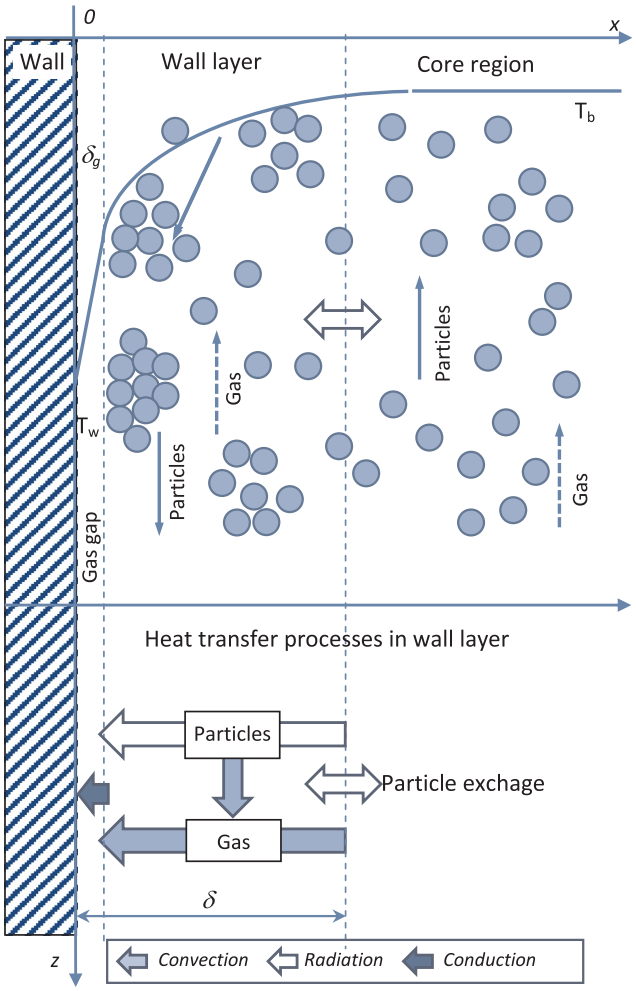

Fig. 2. Schematic solid pattern and heat transfer processes along the wall inside a fluidization column [29–30].

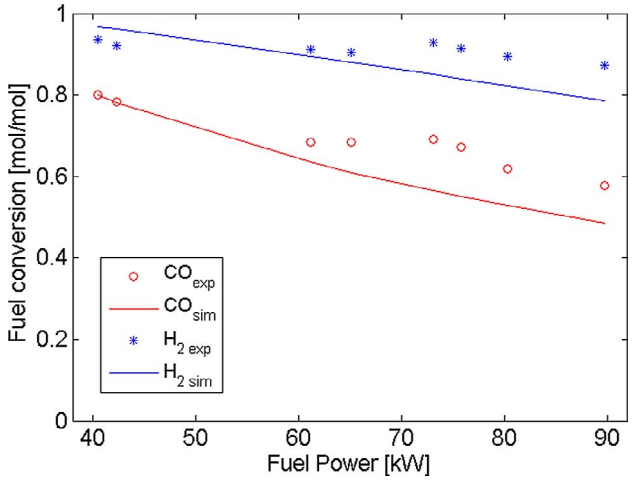

Fig. 3. Model validation against 120 KW CLC unit from Vienna University of Technology [44].

be calculating using the following relation [20]:

$$a = \frac{6\cdot(1-\varepsilon)}{d_p} \tag{24}$$

Two phases can be distinguished while describing the bed-wall heat flux (Eq. (25)): packets (clusters) and lean particle phase. Packets

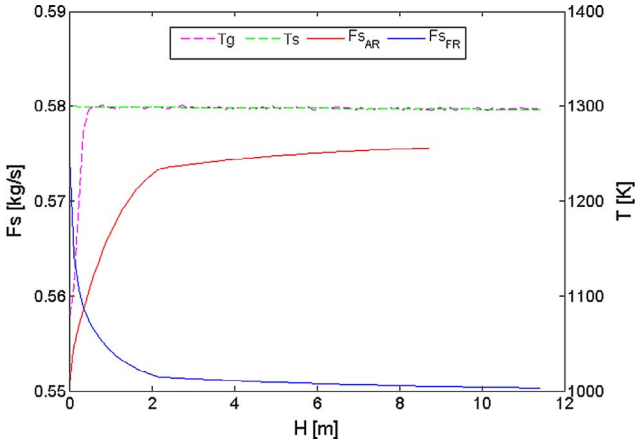

Fig. 4. Oxygen carrier flows in air and fuel reactors.

Table 4
The influence of oxygen carrier to fuel ratio.

Oxygen-carrier to fuel ratio [−]	Conversion [mol%]		
	CO	CH_4	H_2
0.63	27	79	76
1.24	61	89	97
1.76	80	81	99
2.72	94	92	~100

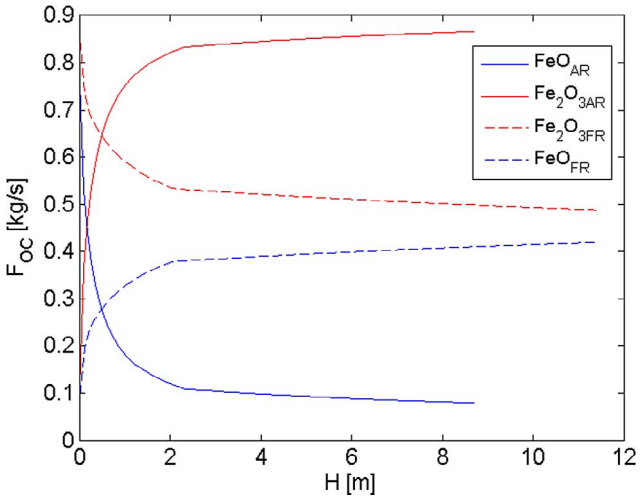

Fig. 5. Oxygen carrier loop inside the CLC system.

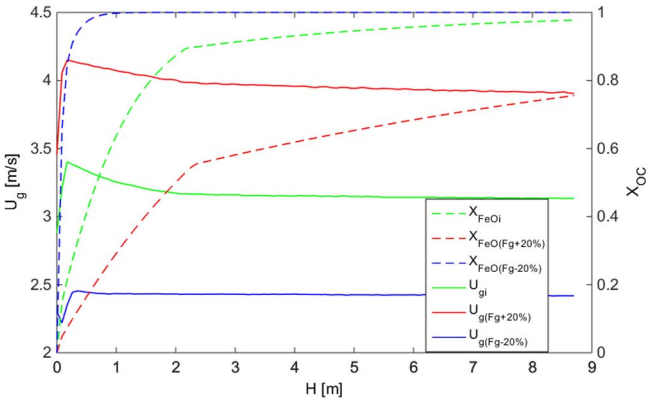

Fig. 6. Distribution of gas velocity in the air reactor.

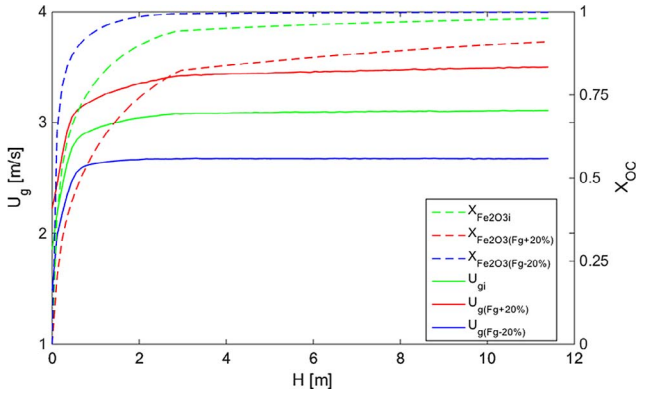

Fig. 7. Gas velocity and conversion dependence in the fuel reactor.

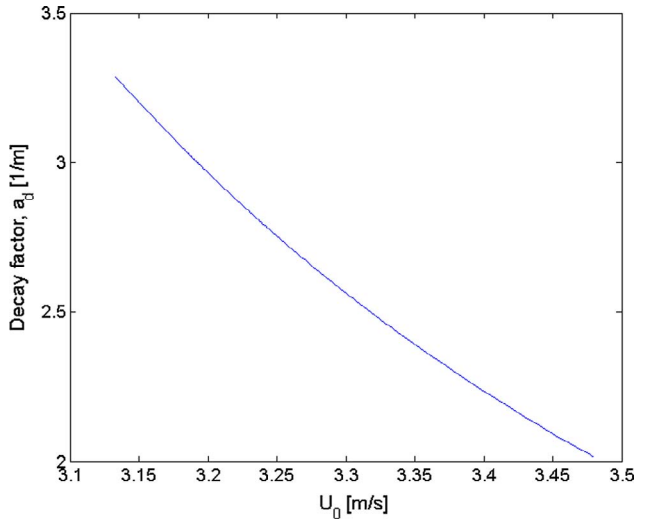

Fig. 8. Decay constant.

exchange heat with the wall through a thin gas film by convection/conduction, according to the classical theory of Mickley and Fairbanks (1955) [33], while the lean phase mainly exchanges heat by gas convection and radiation as presented by Basu and Nag (1996) [34]. f_c

$$H_{pw} = h_{pw}\cdot a_w\cdot(T_p - T_w) \tag{25}$$

$$h_{pw} = f_c\cdot(h_c + h_{rc}) + (1-f_c)\cdot(h_l + h_{rl}) \tag{26}$$

A very important parameter in assessing the heat transfer rate between the particles and the wall is the fraction of surface covered by moving packets, f_c. In order to calculate, a correlation proposed by Golriz and Grace (2002) [35–37], that takes into account the effect of the column diameter in large units, was used.

$$f_c = 1 - exp\left\{-25000\cdot\left[1 - \frac{2}{\exp(0.5\cdot D) + \exp(-0.5\cdot D)}\right]\cdot(1-\varepsilon)\right\} \tag{27}$$

The packets (clusters) convection heat transfer coefficients, h_c, can be expressed using Eq. (28) [28]:

$$h_c = \frac{1}{\left(\frac{4\cdot k_c\cdot\rho_c\cdot Cp_c}{\pi\cdot t_c}\right)^{0.5} + h_w} \tag{28}$$

where

$$k_c = k_g\cdot\left(1 + \frac{(1-\varepsilon_c)\cdot(1-k_g/k_p)}{k_g/k_p + 0.28\cdot\varepsilon_c^{0.63\cdot(k_g/k_p)^{0.18}}}\right) + 0.1\cdot\rho_g\cdot Cp_g\cdot d_p\cdot U_{mf} \tag{29}$$

$$\rho_c = (1-\varepsilon_c)\cdot\rho_p + \varepsilon_c\cdot\rho_g \tag{30}$$

$$Cp_c = (1-\varepsilon_c)\cdot Cp_p + \varepsilon_c\cdot Cp_g \tag{31}$$

$$\varepsilon_c = 1 - 1.23\cdot(1-\varepsilon)^{0.54} \tag{32}$$

For the estimation of the cluster residence time, t_c, the ratio between the mean distance a cluster falls along the wall before it is displaced, L_c, and the cluster downwards velocity, U_c, described in the following expression can be used [38–40]:

$$t_c = \frac{L_c}{U_c} = \frac{0.0178\cdot\rho_{susp}^{0.596}}{0.75\cdot\sqrt{\frac{\rho_p}{\rho_g}\cdot g\cdot d_p}} \tag{33}$$

Suspension density of the bed, ρ_{susp}, was calculated using Eq. (34) [32]:

$$\rho_{susp} = (1-\varepsilon)\cdot\rho_p + \varepsilon\cdot\rho_g \tag{34}$$

A thin gas gap, having a thickness δ_g, is located between the wall and the packets, acting like a conduction resistance to the heat transfer, h_w, given by Eq. (35) [28].

$$h_w = \frac{k_g}{d_p\cdot\delta_g} \tag{35}$$

$$\delta_g = 0.028\cdot(1-\varepsilon)^{-0.59} \tag{36}$$

When the lean particle phase comes in contact with the wall, heat is transferred by gas convective mechanism, according to the following equation [28]:

$$h_l = \frac{k_g\cdot Cp_p}{d_p\cdot Cp_g}\cdot\left(\frac{\rho_l}{\rho_p}\right)^{0.3}\cdot\left(\frac{U_t^2}{g\cdot d_p}\right)^{0.21}\cdot Pr \tag{37}$$

with

$$\rho_l = (1-Y)\cdot\rho_g + Y\cdot\rho_p \tag{38}$$

$$Y = 0.001\% \tag{39}$$

Radiative heat exchange can be treated in a simplified manner considering the exchange between opaque grey media, in this case the particles and the wall, separated by an inert medium, here gas. Thus, the following relation can be used:

$$h_r = \frac{q_r}{T_s - T_w} = \frac{\sigma\cdot(T_s^4 - T_w^4)}{(T_s - T_w)\cdot\left[1 + \frac{1-e}{e} + \frac{1-e_w}{e_w}\right]} \tag{40}$$

In describing the radiative heat transfer coefficients of the clusters h_{rc}, and of the lean phase, h_{rl}, the emissivity, e, in Eq. (40), is replaced with the specific emissivity of the phase: e_c and e_l which can be evaluated using Eqs. (41) and (42) respectively [41,42].

$$e_c = 0.5\cdot(1 + e_p) \tag{41}$$

$$e_l = \left[\frac{e_p}{0.5\cdot(1-e_p)}\cdot\left(2 + \frac{e_p}{0.5\cdot(1-e_p)}\right)\right]^{0.5} - \frac{e_p}{0.5\cdot(1-e_p)} \tag{42}$$

The specific area of the wall, a_w can be estimated from Eq. (43):

$$a_w = \frac{4\cdot(1-\varepsilon_c)}{D} \tag{43}$$

3. Results and discussions

The partial differential equations of the model have been transformed into differential equations by space discretization using first order approximation, and all mathematical equations used have been implemented in Matlab (2013 version). The models developed for the air and fuel reactors have been inter-connected in Simulink (2013 version) and used to simulate the stationary and dynamic behaviors of the CLC unit with the design and operating parameters listed in Table 2.

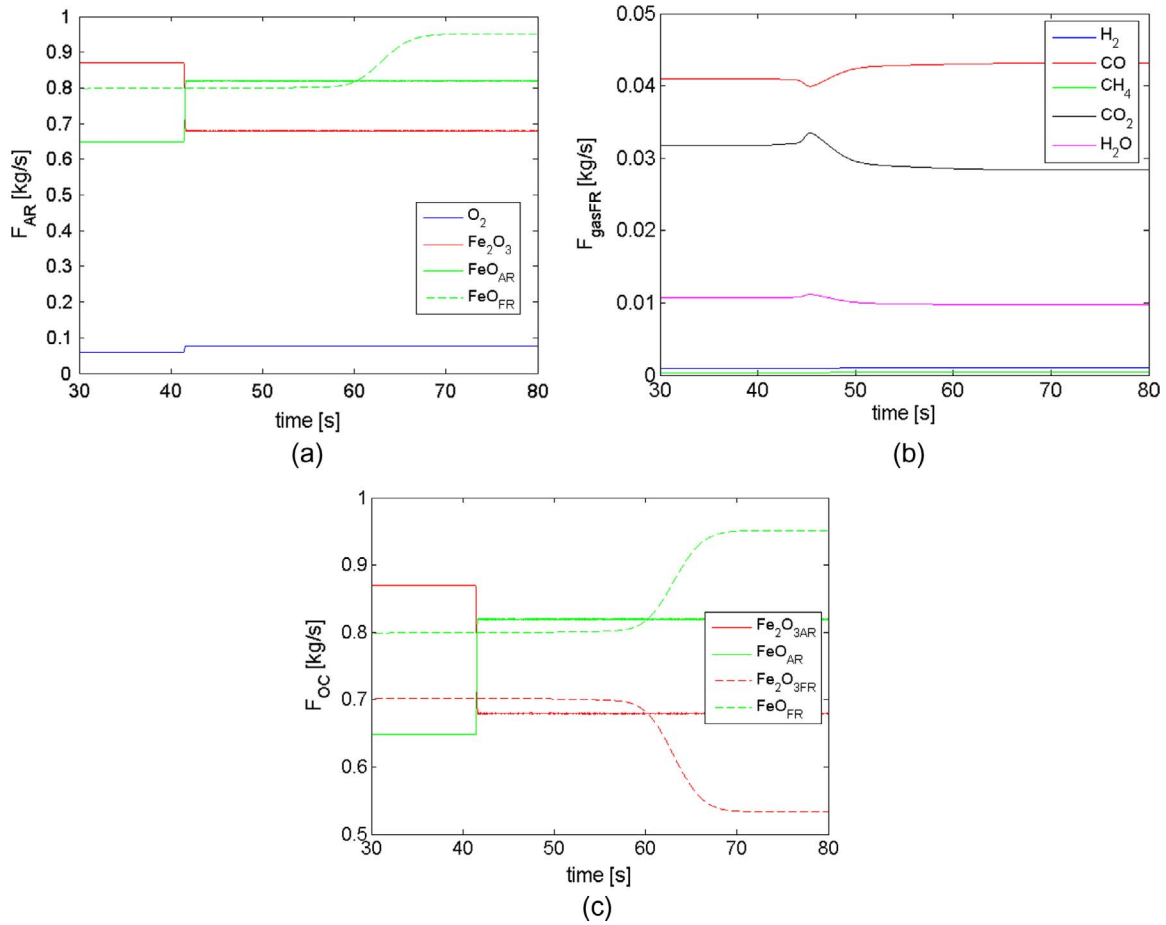

Fig. 9. Dynamic response to a step type signal change. a) Oxygen carrier flow between reactors, at +20% F_g. b) Fuel reactor gas flows, at +20% F_g. c) Oxygen carrier flow between reactors, at −20% F_g.

For the fuel reactor a typical syngas obtained from coal that contains 25–30% H_2 (v/v), 30–60% CO (v/v), 5–15% CO_2 (v/v) and 2–3% H_2O with a small amounts of 1% CH_4 and inert gas N_2 was used as fuel [43].

The simulation results for the 1 MW_{th} syngas-based chemical looping combustion process using ilmenite as oxygen carrier are in line with literature data (e.g. the variation of conversion rate for carbon monoxide is less than 0.5% between simulated and experimental data reported in the literature [9]). For validation, the model developed in this work was simulated in similar condition of the 120 KW CLC unit operated at Vienna University of Technology [44]. The experimental tests were run on ilmenite as oxygen carrier and an equimolar mixture of CO and H_2 as fuel. The simulation results showed good agreement with the experimental ones as it can be seen from Fig. 3, with a maximum deviation of 18% for CO conversion and 10% for the conversion of H_2.

Fig. 4 shows the oxygen carrier flows in and out of the two looping reactors including the inert species, TiO_2 for oxygen carrier to fuel ratio of 0.63. The influence of the oxygen carrier to fuel ratio, on the fuel conversion was investigated. It was observed that increasing the solid inventory leads to an increase in syngas conversion, full H_2 conversion was observed for an oxygen carrier to fuel ratio higher than 1.70 while very small conversion of CO were obtained in case of low oxygen carrier to fuel ratio. The obtained results are listed in Table 4.

In Fig. 5 it is shown more clearly the oxidation/reduction cycles performed by the oxygen carrier considering an oxygen carrier to fuel ratio of 1.76. In the air reactor, FeO is oxydized to Fe_2O_3 which in turn is reduced back to FeO in the fuel reactor and a new loop begins. As it can be seen, the gas and solid bulk temperatures are almost constant in the main part of both reactors (this can be expected considering the perfectly mixed regime in core zone of reactors). Regarding the solid mass flows, the flow inside the fuel reactor is reduced considering the mass losses of the oxygen carrier (oxygen transfer for fuel oxidation). The solid mass flow profile in the air reactor is showing an increase due to the mass gain during the oxygen carrier reoxidation. The reactions are taking part mainly in the dense zone of both reactors (having a height of about 2 m) then the profiles are almost constant.

The gas velocity is a very important parameter influencing the performance of the chemical looping reactors. As seen from Figs. 6 and 7, increasing the gas flow leads to an increase in velocity which also means a more intensified fluidization. As a consequence, the oxygen carrier conversion rate is decreasing due to the fact that the residence time is decreasing. For instance, in case of the air reactor (Fig. 6), the ± 20% variation in the inlet gas flowrate implies an important variation of the oxygen carrier conversion: 100% for lower gas flow and 78% for higher gas flow (the nominal conversion rate is 98%). In case of the fuel reactor (Fig. 7), the ± 20% variation in the inlet gas flowrate implies an important variation of the oxygen carrier conversion: 100% for lower gas flow and 88% for higher gas flow (the nominal conversion rate is 98%).

The decay factor, a_d, expresses the decay of solids fraction with the height. The variation of the decay factor vs. fluidizing velocity is presented in Fig. 8. As it can be seen, the decay factor is rapidly decreasing when the fluidizing velocity is increased (about 1.62 times for a variation of the fluidizing velocity by about 0.5 m/s).

Variations with time of the gaseous components present in the fuel reactor are represented in the Figs. 9 and 10. When a disturbance, step or ramp, is applied to the system, like the increase of the fluidizing gas flow by 20%, the system's response is very fast and a new steady state is

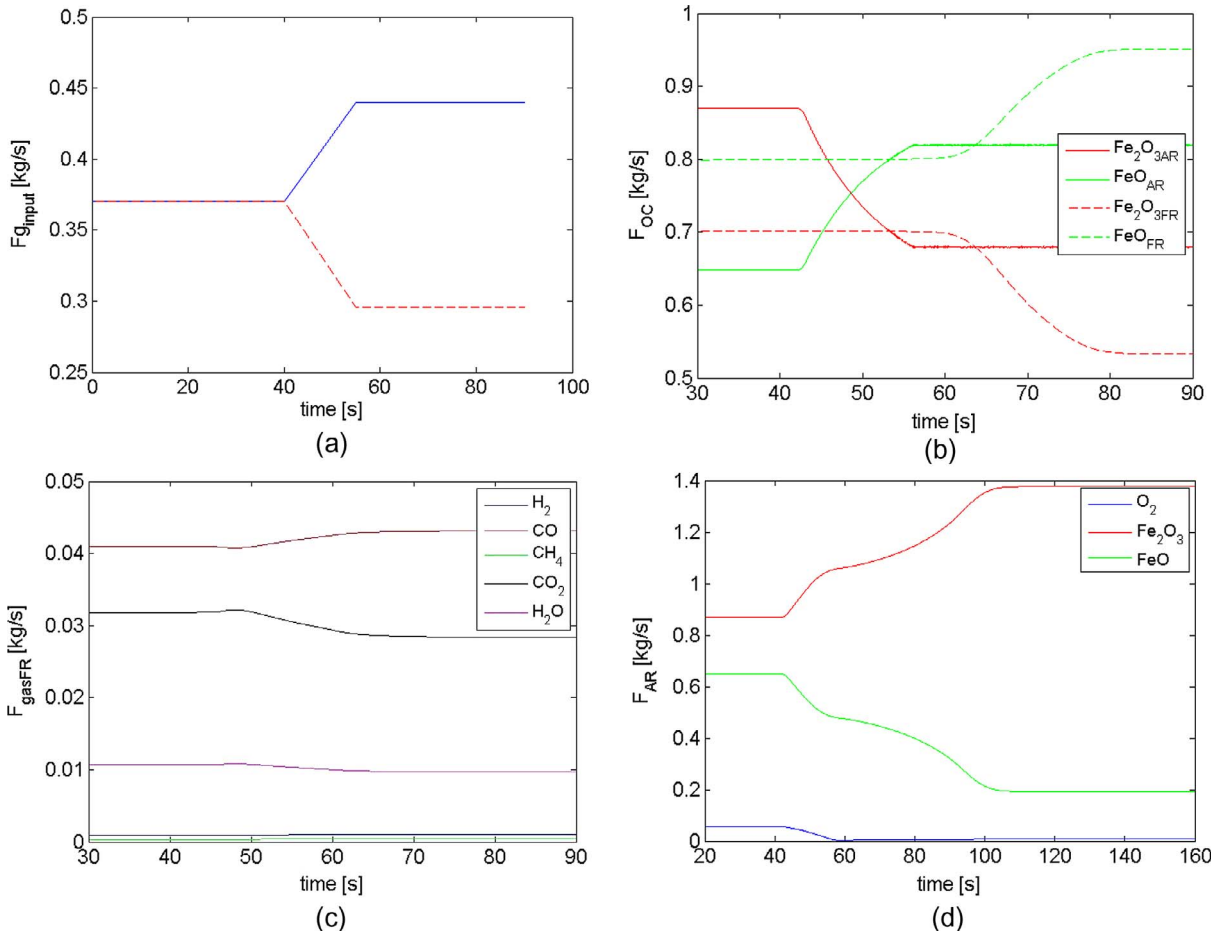

Fig. 10. Dynamic response to a ramp type signal change. a) Input gas flow ramp change. b) Oxygen carrier flow between reactors at +20% F_g. c) Fuel reactor gas flows, at +20% F_g. d) Oxygen carrier flow between reactors, at −20% F_g.

achieved as seen in Fig. 9.

As it can be noticed from Fig. 9, a step increase of the input gas flow implies an increase of the fluidization velocity and as a consequence the residence time in the reactor is reduced as well as the conversion rates in both reactors. For instance, a step increase of the input gas flow with 20% triggers a proportional increase of 20% of the oxygen carrier flowrate in the air reactor (from 0.65 kg/s to 0.82 kg/s) and a slight decrease of fuel conversion (Fig. 9b). The 20% step decrease induces a similar behavior like the increase but in opposite direction and in this case a slower response of the system was observed (see Fig. 9c). Another important conclusion regarding the dynamic response of the process is that the air reactor responds very quickly to the step perturbation of the input gas flow while the fuel reactor is significantly slower in reaching a new steady state condition (the perturbation is delayed from the air reactor to the fuel reactor). This conclusion is valid for both solid and gas flows.

As it can be noticed from Fig. 10, the 20% ramp increase of the input gas flow implies a slower response of the system in comparison to the 20% step increase. The new steady state conditions are similar with the case of the step change. The 20% ramp decrease induces a similar behavior like the increase but in opposite direction (similar with step change). In both ramp situations (either increase or decrease), the conversion rate is more affected in the air reactor that the fuel reactor (e.g. 62% vs. 40% in case of 20% ramp decrease).

As important overall conclusion of this work is that the dynamic behavior of syngas-based chemical looping system is quick, noting a slight delay in case of the fuel reactor in comparison to the air reactor. This situation is for the case of inlet gas flow modification for the air reactor. In term of oxygen carrier conversion rate, the modification of the gas flow induces a higher variation rate in the case of air reactor in comparison to the fuel reactor.

4. Conclusions

The most used configuration for chemical looping combustion of gaseous fuels (syngas was considered in this work) consists of two interconnected fluidized bed columns. The mathematical modeling and simulation of interconnected chemical looping combustion columns is required for the design, optimization and most importantly their scale-up to be commercially viable. A dynamic mathematical model has been developed to simulate a 1 MW_{th} syngas-based fluidized bed chemical looping combustion process with iron based oxygen carrier (ilmenite). The mass and energy balance equations, for interconnected fluidized bed reactors together with the equations that describe the hydrodynamics and heat transfer processes were implemented in MATLAB/Simulink. The developed model was used to predict (in space and time): gas and solid velocity distribution, gas composition distribution, behavior of oxygen carrier, and temperature profiles inside the air and fuel reactor.

The dynamic behavior of the syngas-based chemical looping combustion process was studied by step and ramp input changes of the gas flow rate in the air reactor. For instance, a step increase of the input gas flow with 20% triggers a proportional increase of the oxygen carrier flowrate in the air reactor, reducing correspondently the oxygen carrier conversion rate. Another important finding is that in case of ramp variations, the conversion rate is more affected in the air reactor that the fuel reactor. The developed dynamic model is of great importance for overall process optimization in the dynamic operation scenario (as

required in modern energy system) as well as set-up of process control algorithm.

Acknowledgments

This work was supported by a grant of Ministry of Research and Innovation, CNCS–UEFISCDI, project number PN-III-P4-ID-PCE-2016-0031: "*Developing innovative low carbon solutions for energy-intensive industrial applications by Carbon Capture, Utilization and Storage (CCUS) technologies*" within PNCDI III and a scholarship no. 34829-1/2016 awarded by Babeș-Bolyai University.

References

[1] IPCC, Climate Change 2007: Adaptation and vulnerability. Fourth assessment report of the Intergovernmental Panel on Climate Change; 2007.
[2] Nandy A, Loha C, Gu S, Sarkar P, Karmakar MK, Chatterjee PK. Present status and overview of chemical looping combustion technology. Renew Sust Energy Rev 2016;59:597–619.
[3] Ishida M, Zheng D, Akehata T. Evaluation of a chemical-looping combustion power-generation system by graphic energy analysis. Energy 1987;12:147–54.
[4] Hossain MM, de Lasa HI. Chemical-looping combustion (CLC) for inherent CO2 separations – a review. Chem Eng Sci 2008;63:4433–51.
[5] Adanez J, Cuadrat A, Abad A, Gayan P, de Diego L, Garcia-Laabiano F. Ilmenite activation during consecutive redox cycles in chemical-looping combustion. Energy Fuels 2010;24:1402–13.
[6] Adanez J, Abad A, Garcia-Labiano F, Gayan P, de Diego LF. Progress in chemical-looping combustion and reforming technologies. Prog Energy Combust Sci 2012;38:215–82.
[7] Lyngfelt A, Leckner B, Mattisson T. A fluidized-bed combustion process with inherent CO2 separation: application of chemical-looping combustion. Chem Eng Sci 2001;56:3101–13.
[8] Parker J. CFD model for the simulation o fchemical looping combustion. Powder Technol 2014;265:47–53.
[9] Abad A, Gayan P, de Diego LF, Garcia-Labiano F, Adanez J. Fuel reactor modelling in chemical-looping combustion of coal: 1. Model formuation. Chem Eng Sci 2013;87:277–93.
[10] Cormos AM, Chisalita DA. Contribution to the modeling and simulation of the iron-based chemical looping combustion process. Energy Technol 2016;4:1179–87.
[11] Ströhle J, Orth M, Epple B. Design and operation of a 1 MWth chemical looping plant. Appl Energy 2014;113:1490–5.
[12] Borowiec K, Rosenqvist T. Phase relations and oxidation studies in the system Fe-Fe2O3-TiO2 at 700–1000 degree C. Scand J Metall 1981;10:217–24.
[13] Itoh S, Sato S, Ono J, Okada H, Nagasaka T. Feasibility study of the new rutile extraction process from natural ilmenite ore based on the oxidation reaction. Metal Mater Trans 2006;37B:979–85.
[14] Rao DB, Riguard M. Kinetics of the oxidation of ilmenite. Oxid Met 1975;9:99–116.
[15] Adanez J, Cuadrat A, Abad A, Gayan P, de Diego LF, Garcia-Labiano F. Ilmenite activation during consecutive redox cycles in chemical-looping combustion. Energ Fuel 2010;24(1402):1413.
[16] Abad A, Adanez J, Cuadrat A, Garcia-Labiano F, Gayan P, de Diego LF. Kinetics of redox reactions of ilmenite for chemical-looping combustion. Chem Eng Sci 2011;66:689–702.
[17] Donski E, McElwain DLS, Wibberley LJ. Estimation and modeling of parameters for direct reduction in iron ore/coal composites: Part II. Kinetic parameters. Metal Mater Trans 2003;34B:255–66.
[18] Kunii D, Levenspiel O. Circulating fluidized-bed reactors. Chem Eng Sci 1997;52:2471–82.
[19] Johnsson F, Andersson S, Leckner B. Expansion of a freely bubbling fluidized bed. Powder Technol 1991;68:117–23.
[20] Kunii D, Levenspiel O. Fluidization Engineering Second Eddition. Butterworth-Heinemann; 1991, Chapter 3: p. 62, Chapter 6: 146–147, Chapter 7: 176, Chapter 8: p. 200–204.
[21] Broadhurst TE, Becker HA. Onset of fluidization and slugging in beds of uniform particles. AIChE J 1975;21:238–47.
[22] Shresthaa S, Alia BS, Jana BM, Limb TM, Sheikh KE. Hydrodynamic properties of a cold model of dual fluidized bed gasifier: a modeling and experimental investigation. Chem Eng Res Des 2016;109:791–805.
[23] Pallares D, Johnsson F. Macroscopic modelling of fluid dynamics in large-scale circulating fluidized beds. Prog Energy Combust Sci 2006;32:539–69.
[24] Zenz FA, Weil NA. A theoretical-empirical approach to the mechanism of particle entrainment from fluidized beds. AIChE J 1958;4:472–9.
[25] Loffler G, Kaiser S, Bosch K, Hofbauer H. Hydrodynamics of a dual fluidized-bed gasifer—Part I: simulation of a riser with gas injection and difuser. Chem Eng Sci 2003;58:4197–213.
[26] Adanez J, Gayan P, Garcia-Labiano F, Diego L. Axial voidage profiles in fast fiuidized beds. Powder Technol 1994;81:259–68.
[27] Gunnarsson A. MSc: process simulation of a 1 MWth chemical looping pilot plant with coal and biomass as fuel. Gothenburg: Chalmers University of Technology; 2014.
[28] Scala F. Chapter 5: Heat and mass transfer in fluidized bed combustion and gasification systems. Fluidized bed technologies for near-zero emission combustion and gasification. Cambridge, UK: Woodhead Publishing Limited; 2013. p. 177-253.
[29] Blaszczuk A, Nowak W. Bed-to-wall heat transfer coefficient in a supercritical CFB boiler at different bed particle sizes. Int J Heat Mass Transfer 2014;79:736–49.
[30] Xie D, Bowen BD, Grace JR, Lim CL. Two dimensional model of heat transfer in circulating fluidized bed. Part I: model development and validation,". Int J Heat Mass Transfer 2003;46:2179–91.
[31] Makkawi Y. Particle to Gas Heat Transfer in a Circulating Fluidized Bed Riser. 10th International Conference on Circulating Fluidized Beds and Fluidization Technology - CFB-10, T. Knowlton; 2013.
[32] Abdelmotalib HM, Youssef MA, Hassan AA, Youn SB, Im IT. Heat transfer process in gas–solid fluidized bed combustors: a review. Int J Heat Mass Transfer 2015;89:567–75.
[33] Mickley HS, Fairbanks DF. Mechanism of heat transfer to fluidized beds. AIChE J 1955;1:374–84.
[34] Basu P. Heat transfer to walls of a circulating fluidized-bed furnace. Chem Eng Sci 1996;51:1–26.
[35] Golriz MR, Grace JR. Predicting heat transfer in large-scale CFB boilers. In: 7th International conference on circulating fluidized beds, Niagara Falls, Canada; 2002.
[36] Dutta A, Basu P. An improved cluster-renewal model for the estimation of heat transfer coefficients on the furnace walls of commercial circulating fluidized bed boilers. J Heat Transfer 2004;126:1040–3.
[37] Brems A, Cáceres C, Dewil R, Baeyens J, Pitié F. Heat transfer to the riser-wall of a circulating fluidised bed (CFB). Energy 2013;50:493–500.
[38] Lints M, Glicksman L. Parameters governing particle-to-wall heat transfer in a circulating fluidized bed. Circulating Fluidized Bed Technology IV. American Institute of Chemical Engineers, New-York, A. Avidan; 1994, p. 297–304.
[39] Wu RL, Grace JR, Lim CJ. A model for heat transfer in circulating fluidized beds. Chem Eng Sci 1990;45:3389–98.
[40] Noymer PD, Glicksman LR. Descent velocities of particle clusters at the wall of a circulating fuidized bed. Chem Eng Sci 2000;55:5283–9.
[41] Grace J. Fluidized bed heat transfer. Handbook of Multiphase Flow, McGraw-Hill, Hempshire, Washington, DC, G. Hesrtoni; 1982, p. 9–70.
[42] Brewster M. Effective absorptivity and emissivity of particulate media with application to a fluidized bed. J Heat Transfer 1986;108:710–3.
[43] Mondal P, Dang GS, Garg MO. Syngas production through gasification and cleanup for downstream applications — Recent developments. Fuel Process Technol 2011;92:1395–410.
[44] Pröll T, Mayer K, Bolhàr-Nordenkampf J, Kolbitsch P, Mattisson T, Lyngfelt A, et al. Natural minerals as oxygen carriers for chemical looping combustion in a dual circulating fluidized bed system. Energy Proc 2009;1:27–34.